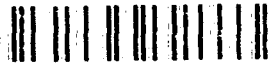AD-A270 852

ARMY RESEARCH LABORATORY

Focused-Ion-Beam Material Removal Rates

by Bruce Geil

ARL-MR-114   September 1993

93-25165

REPORT DOCUMENTATION PAGE

1. AGENCY USE ONLY *(Leave blank)*	2. REPORT DATE	3. REPORT TYPE AND DATES COVERED
	September 1993	Summary, January 1991–present

4. TITLE AND SUBTITLE	5. FUNDING NUMBERS
Focused-Ion-Beam Material Removal Rates	PE: 91A

6. AUTHOR(S)

Bruce Geil

7. PERFORMING ORGANIZATION NAME(S) AND ADDRESS(ES)	8. PERFORMING ORGANIZATION REPORT NUMBER
U.S. Army Research Laboratory Attn: AMSRL-WT-NG 2800 Powder Mill Road Adelphi, MD 20783-1197	ARL-MR-114

9. SPONSORING/MONITORING AGENCY NAME(S) AND ADDRESS(ES)	10. SPONSORING/MONITORING AGENCY REPORT NUMBER
U.S. Army Research Laboratory 2800 Powder Mill Road Adelphi, MD 20783-1197	

11. SUPPLEMENTARY NOTES

AMS code: 611101.91A
ARL PR #: 1AE523

12a. DISTRIBUTION/AVAILABILITY STATEMENT	12b. DISTRIBUTION CODE
Approved for public release; distribution unlimited.	

13. ABSTRACT *(Maximum 200 words)*

Focused-ion-beam milling is a tool used in failure analysis and production of integrated circuits. This technique uses a focused gallium beam to mill away materials on a surface. Each material mills at a different rate, which must be experimentally determined. The data presented here for several materials used in standard integrated circuit processes will allow the user to determine the dose level needed to mill a certain amount of a given material.

14. SUBJECT TERMS	15. NUMBER OF PAGES
Focused ion beam, material removal rates	20
	16. PRICE CODE

17. SECURITY CLASSIFICATION OF REPORT	18. SECURITY CLASSIFICATION OF THIS PAGE	19. SECURITY CLASSIFICATION OF ABSTRACT	20. LIMITATION OF ABSTRACT
Unclassified	Unclassified	Unclassified	UL

Contents

Page

Figures

Tables

3

1. Introduction

Focused-ion-beam (FIB) systems have been used for several years in failure analysis of integrated circuits and the repair of photomasks. For integrated-circuit failure analysis, the FIB is used for the selective removal of materials (known as "milling") in areas of the circuit, so that the circuit cross sections can be examined. The problem with milling through an integrated circuit is that the mill rates vary for the many different kinds of materials used in semiconductor processing. If the rate at which a material mills is unknown, one cannot accurately calculate mill depths. We performed the work described here to study the material removal rates of different microelectronic device materials.

An FIB system is composed of three major components: a vacuum system, electronics systems, and an ion-beam column. The ion column has two major components. The first component is the gallium source, which is a small Y-shaped wire. The gallium is stored at the center of the Y and the ions are pulled off of the base of the Y. Once the ions are pulled off the source, they are accelerated to 25 keV, focused, and stigmated through the remainder of the column. The second major component of the column is the electronics required to steer the ion beam over the sample. When the ions hit the sample, the kinetic energy of the impact knocks ions off the sample, thus forming a cavity in the sample. This cavity can be as small as $0.5~\mu m^2$ or as large as $80~\mu m^2$.

The data obtained in milling these materials have been used for various programs. We used the FIB to study the etch profile of silicon dioxide for production of quantum wires. These wires were used by the University of Maryland to study quantum effects in stressed gallium arsenide. In a U.S. Army project to develop optical integrated circuits, we used these data to determine the proper depth and time for milling waveguide facets. We also used these data in a Navy program to develop a semiconductor ignitor,[1] to determine the etch profile of a silicon dioxide layer buried under two other levels of material. For this program it was very important that the circuit levels underneath the silicon dioxide not be damaged during the milling.

2. Method

In this study, the FIB system used was a Micrion 808 mask repair system. This fully automated system uses gallium ions as described above to mill the material. The system has a beam spot size of 200 nm at 25 keV of extraction voltage. The extraction voltage determines the power of the beam: if the voltage is increased, the ions will strike the surface with higher kinetic energy. This can cause problems when one is trying to mill material, since the higher energy causes the ions to tunnel into the material instead of removing it. The beam current varies between 366 pA, when a new aperture is being used, and approximately 450 pA as the aperture in

[1] J. McCullen, J. Terrell, and R. Reams, *Electrical Characterization of a Semiconductor Primer Ignitor Chip for Ammunition*, Harry Diamond Laboratories, HDL-TM-92-13 (July 1992).

the system ages. The aperture increases in size as the beam passes through it, which increases the beam size and the amount of current that passes through the aperture. The system monitors this current during the milling process so changes in the current do not affect the dose being applied to a given area. The increase in current reduces the time required to apply the dose to the area, thus increasing the milling rate. The beam is scanned over the designated area using a dwell time of 300 μs per pixel with an overlap of 160 nm for every pixel. The largest area that can be milled is an 80- × 80-μm field. Areas any larger than this cause a decrease in the overlap of the pixels, thus changing the mill rate and resulting in a more ragged cavity. Both the dwell time and the pixel overlap are adjustable to compensate for machine variations. Adjustment of the dwell time can also reduce the amount of gallium implanted into the substrate during the milling process.

In this program, we studied various materials used in semiconductor processing, specifically, gallium arsenide, single crystalline polysilicon, 28-percent aluminum gallium arsenide, thermally grown silicon dioxide, both evaporated and e-beam deposited aluminum, barium titanate, sputtered and evaporated gold, silicon carbide, and silicon nitride. We applied these materials to a silicon substrate except for the samples of gallium arsenide and aluminum gallium arsenide, which we milled in solid form. After we deposited each material, we etched away a small area using either wet or plasma etch techniques. We then used a profilometer to determine the initial depth of the material. In all cases, we left at least 1000 Å of material after the FIB mill to prevent any sublayers from affecting the milling rate. We performed all mills in the center of the sample to prevent any edge effects. Once the samples were in position, we milled four 10- × 60-μm boxes into each sample. Figure 1 shows the plot obtained from the profilometer and figure 2 shows how the actual milled areas appear. We milled each one of these boxes using a different dose of ions per square micron. When we completed the milling, we measured the depth of the etched areas using a Tencor Alpha Step 200 profilometer. This profilometer has a resolution of 5 nm in the vertical and 40 nm in the horizontal range. All the measurements on the profilometer were done using the 80-μm scan field at 25 samples per micrometer.
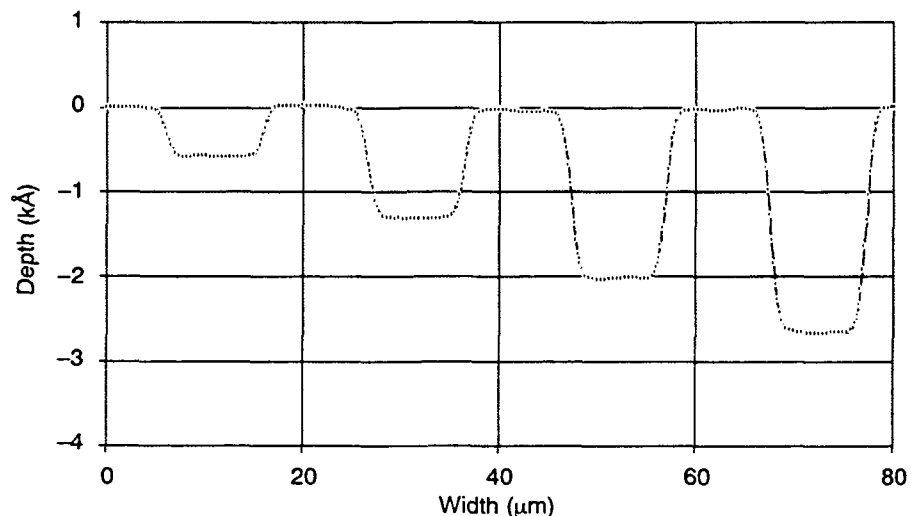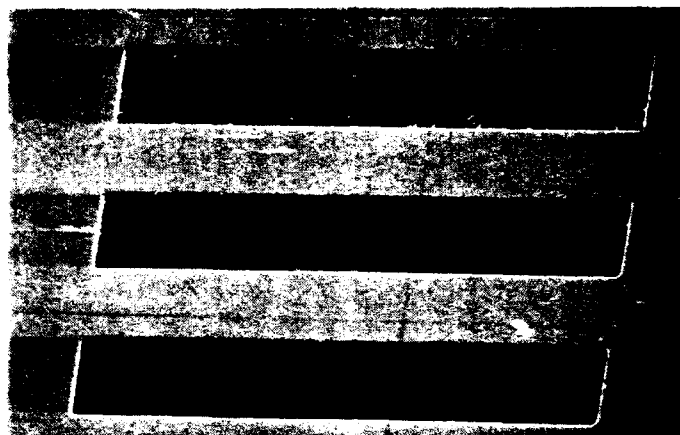
Figure 1. Profile of completed mill.

6

Figure 2. SEM
micrograph of milled
regions.

3. Results

Table 1 shows the raw data which demonstrate the degree of mill rate linearity of various doses of the materials studied. The first column is the area dose in nC/μm^2 that was entered into the FIB system. The second column is the dose converted to ions per square centimeter. The depth in angstroms is the average depth the profilometer calculates using a line-averaging method to average out minor height variations. The next two columns are the calculated values of the mill rate in μm^3/s. This value was calculated using the equation

$$\text{Rate} = \text{amps}/\text{dose} \cdot \text{depth}.$$

Two different values for the current were used to give a range of useful rates for the system dependent on the functional beam current. The current values chosen to calculate this rate are 366 and 450 pA. To check the degree of linearity, a least-squares-fit approximation was applied to each set of dose versus depth data and is shown in table 2. In all cases the returned coefficient of determination was greater than 0.950, which indicates a high degree of linearity. Since a curve fit was done, the values for the slope and y-intercept are also indicated next to the degree of linearity. Figures 3 through 11 show the depth and area dose data plotted with the dose in nC/μm^2 on the x axis and the depth in angstroms on the y axis. Figures 12 through 22 show the area dose and mill rate plotted with the dose in nC/μm^2 on the x axis and the mill rate in μm^3/s on the y axis. The repeatability of these values is within five percent. The repeatability of these data is affected by several parameters including the focus and stigmation of the system during the mill, the ion sputtering rate of the material, and the age of the aperture in the system.

Table 1. Mill rate data.

Dose (nC/μm^2)	Dose (ion/cm^2)	Depth (Å)	Rate 0.366 pA (μm^3/s)	Rate 0.450 pA (μm^3/s)
Gallium arsenide				
0.250	1.56×10^{17}	2445.000	0.35795	0.44010
0.500	3.13×10^{17}	4260.000	0.31183	0.38340
1.000	6.25×10^{17}	8550.000	0.31293	0.38475
1.500	9.38×10^{17}	13270.000	0.32379	0.39810
2.000	1.25×10^{18}	17440.000	0.31915	0.39240
28% aluminum gallium arsenide				
0.250	1.56×10^{17}	1920.000	0.28109	0.34560
0.500	3.13×10^{17}	3560.000	0.26059	0.32040
0.750	4.69×10^{17}	5620.000	0.27426	0.33720
1.000	6.25×10^{17}	7475.000	0.27359	0.33638
1.500	9.38×10^{17}	11440.000	0.27914	0.34320
Polycrystalsilicon				
0.250	1.56×10^{17}	775.000	0.11346	0.13950
0.375	2.34×10^{17}	1135.000	0.11078	0.13620
0.500	3.13×10^{17}	1735.000	0.12700	0.15615
0.750	4.69×10^{17}	2720.000	0.13274	0.16320
1.000	6.25×10^{17}	3385.000	0.12389	0.15233
Silicon dioxide				
0.010	6.25×10^{15}	30.000	0.10980	0.13500
0.020	1.25×10^{16}	60.000	0.10980	0.13500
0.040	2.50×10^{16}	80.000	0.07320	0.09000
0.080	5.00×10^{16}	175.000	0.08006	0.09844
0.125	7.81×10^{16}	375.000	0.10980	0.13500
0.160	1.00×10^{17}	400.000	0.09150	0.11250
0.250	1.56×10^{17}	880.000	0.12883	0.15840
0.375	2.34×10^{17}	1430.000	0.13957	0.17160
0.500	3.13×10^{17}	1840.000	0.13469	0.16560
Silicon carbide				
0.250	1.56×10^{17}	425.000	0.06222	0.07650
0.500	3.13×10^{17}	715.000	0.05234	0.06435
0.750	4.69×10^{17}	1090.000	0.05319	0.06540
1.000	6.25×10^{17}	1510.000	0.05527	0.06795
Barium titanate				
0.500	3.13×10^{17}	500.000	0.03660	0.04500
1.000	6.25×10^{17}	2100.000	0.07686	0.09450
1.500	9.38×10^{17}	3500.000	0.08540	0.10500
Evaporated aluminum				
0.250	1.56×10^{17}	740.000	0.10834	0.13320
0.500	3.13×10^{17}	1190.000	0.08711	0.10710
0.750	4.69×10^{17}	1940.000	0.09467	0.11640
1.000	6.25×10^{17}	2480.000	0.09077	0.11160
Electron-beam deposited aluminum				
0.500	3.13×10^{17}	1070.000	0.07832	0.09630
0.750	4.69×10^{17}	1580.000	0.07710	0.09480
1.000	6.25×10^{17}	2095.000	0.07668	0.09428

Table 1. Mill rate data (cont'd).

Dose (nC/μm^2)	Dose (ion/cm^2)	Depth (Å)	Rate 0.366 pA (μm^3/s)	Rate 0.450 pA (μm^3/s)
Silicon nitride				
0.250	1.56×10^{17}	385.000	0.05636	0.06930
0.500	3.13×10^{17}	900.000	0.06588	0.08100
0.750	4.69×10^{17}	1455.000	0.07100	0.08730
1.000	6.25×10^{17}	2100.000	0.07686	0.09450
Sputtered gold				
0.020	1.25×10^{16}	600.000	1.09800	1.35000
0.040	2.50×10^{16}	1200.000	1.09800	1.35000
0.080	5.00×10^{16}	2100.000	0.96075	1.18125
0.100	6.25×10^{16}	2240.000	0.81984	1.00800
0.125	7.81×10^{16}	2850.000	0.83448	1.02600
0.160	1.00×10^{17}	3500.000	0.80063	0.98438
0.200	1.25×10^{17}	5075.000	0.92873	1.14188
0.300	1.88×10^{17}	7740.000	0.94428	1.16100
Evaporated gold				
0.050	3.13×10^{16}	875.000	0.64050	0.78750
0.075	4.69×10^{16}	950.000	0.46360	0.57000
0.100	6.25×10^{16}	1275.000	0.46665	0.57375
0.150	9.38×10^{16}	1720.000	0.41968	0.51600

Table 2. Data analysis.

Material	Linear-fit dose mill rate (μm$^2 \cdot$Å/nC)	Zero dose depth intercept (Å)	Coefficient of determination	Average mill rate 366 pA (μm^3/s)	Average mill rate 450 pA (μm^3/s)
Gallium arsenide	8689.27	69.27	0.999	0.325	0.400
28% aluminium gallium arsenide	7673.51	–135.81	1.000	0.274	0.337
Polycrystalsilicon	3601.72	–120.99	0.996	0.122	0.149
Silicon dioxide	3838.93	–79.86	0.995	0.109	0.134
Silicon carbide	1452.00	27.50	0.997	0.056	0.069
Barium titanate	3000.00	–966.67	0.999	0.066	0.082
Evaporated aluminum	2388.00	95.00	0.999	0.095	0.117
Electron-beam deposited aluminum	2050.00	44.17	1.000	0.077	0.095
Silicon nitride	2280.00	–215.00	0.999	0.068	0.083
Sputtered gold	25096.49	–52.36	0.986	0.936	1.150
Evaporated gold	8891.43	371.43	0.974	0.498	0.612

Figure 3. Depth
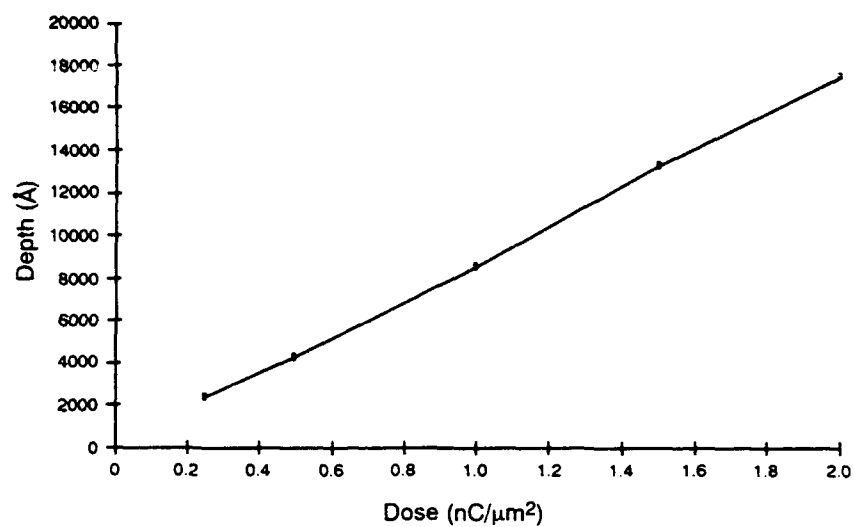versus dose for
gallium arsenide.

Figure 4. Depth
versus dose for 28-
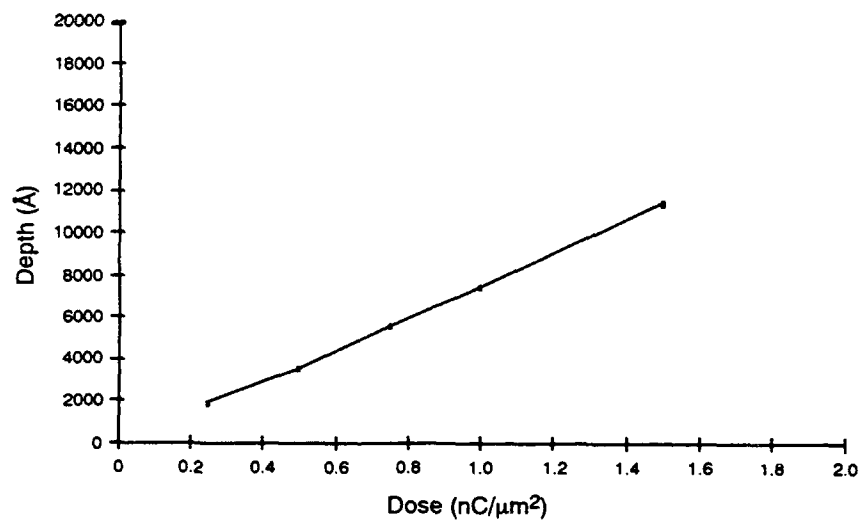percent aluminum
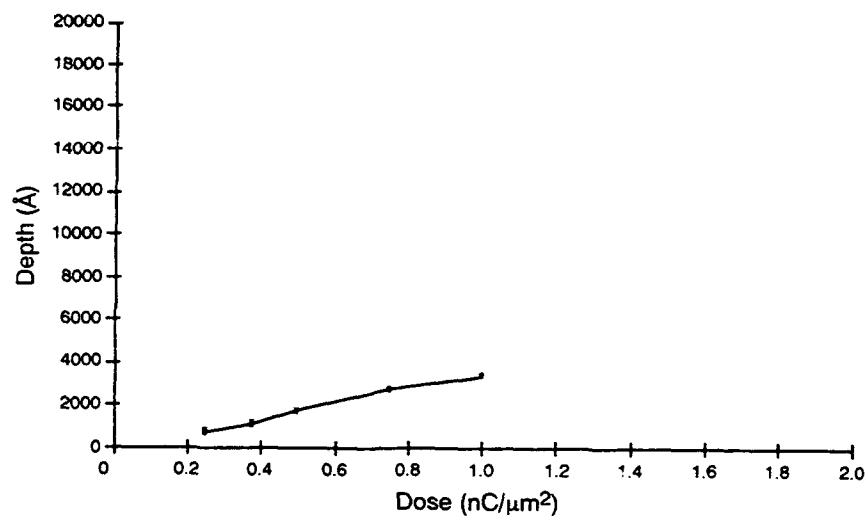gallium arsenide.

Figure 5. Depth
versus dose for
polysilicon.

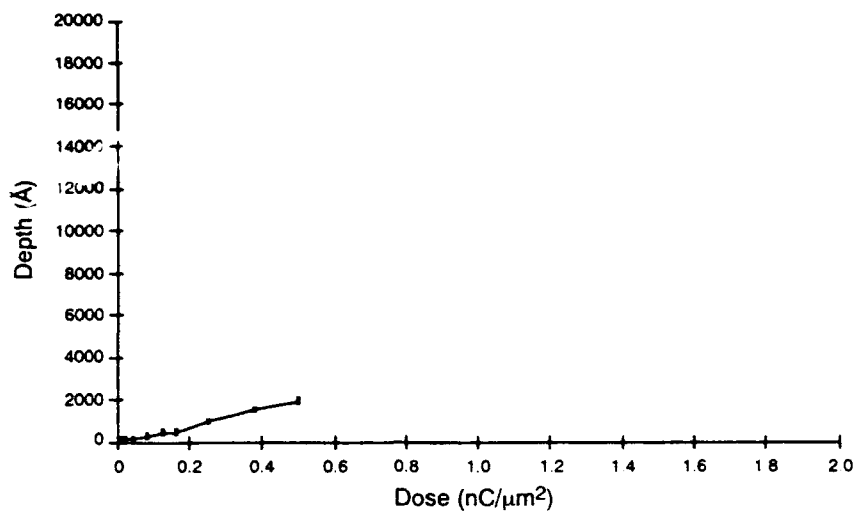**Figure 6. Depth versus dose for silicon dioxide.**

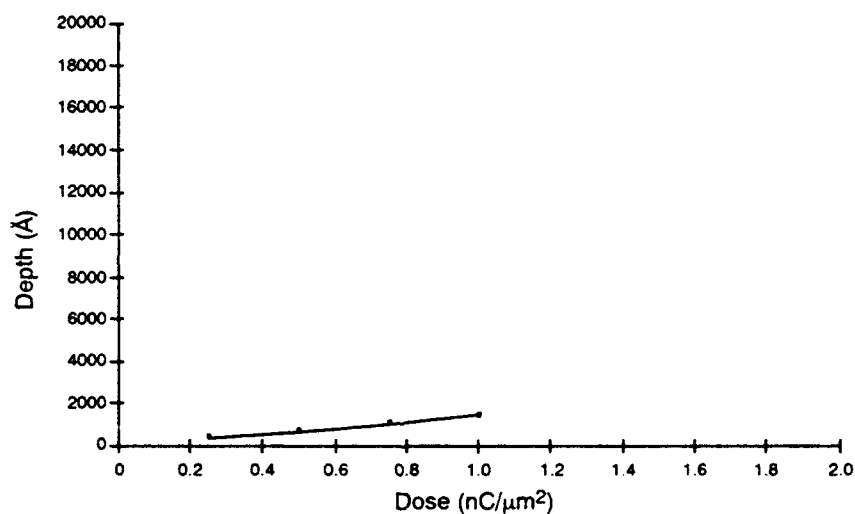**Figure 7. Depth versus dose for silicon carbide.**

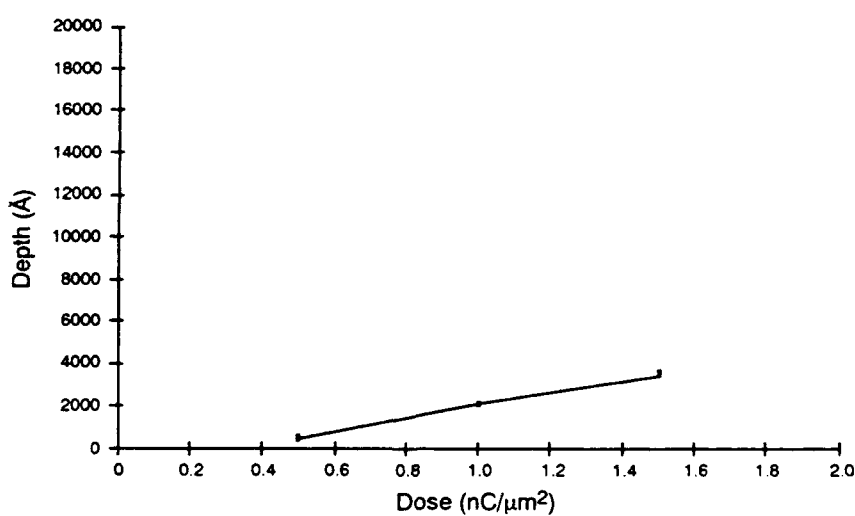**Figure 8. Depth versus dose for barium titanate.**

11

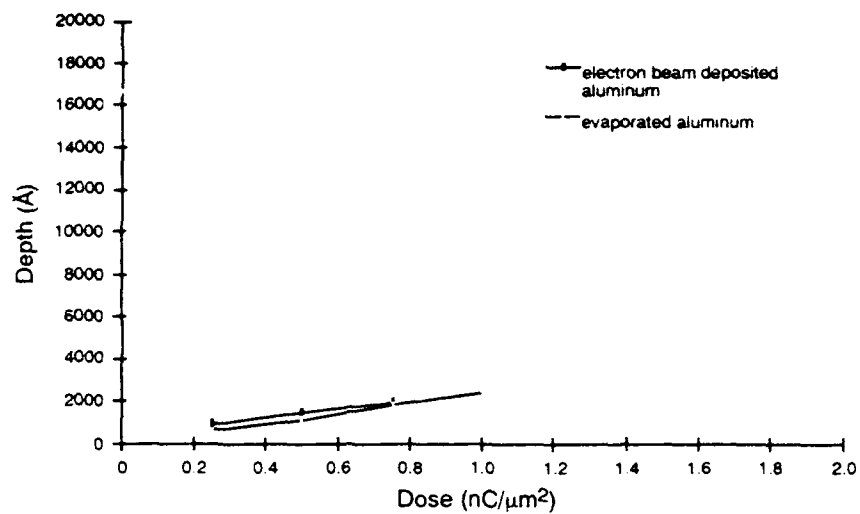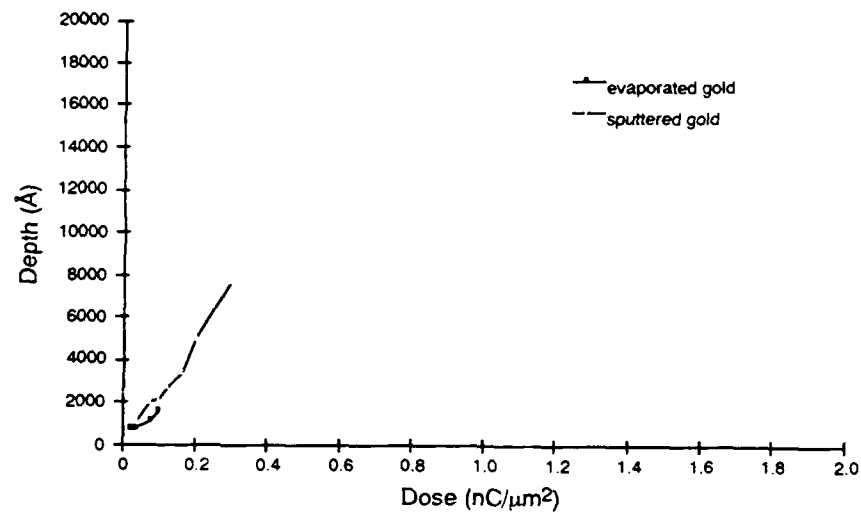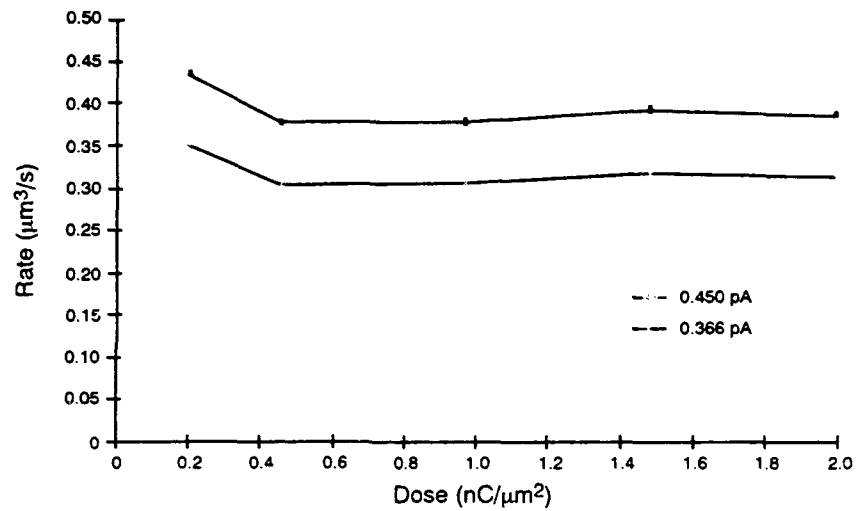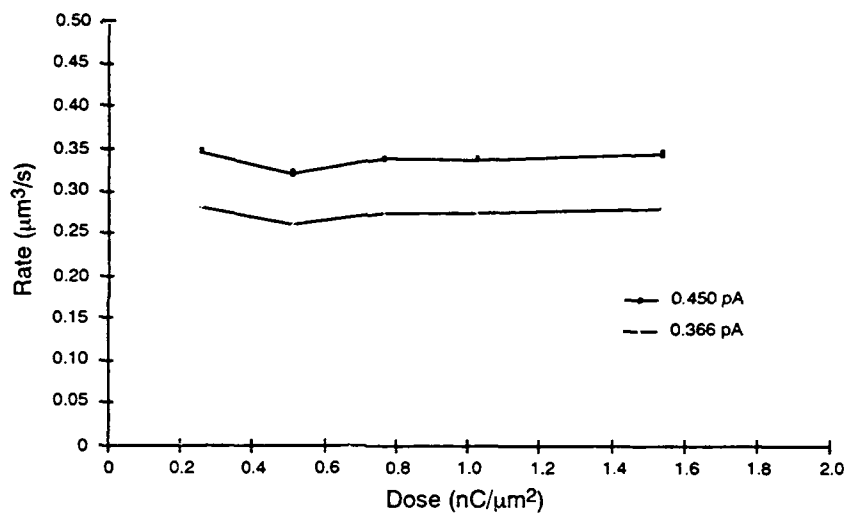**Figure 9. Depth versus dose for aluminum.**

Depth (Å) vs Dose (nC/μm²)

- electron beam deposited aluminum
- evaporated aluminum

Figure 10. Depth versus dose for silicon nitride.

Depth (Å) vs Dose (nC/μm²)
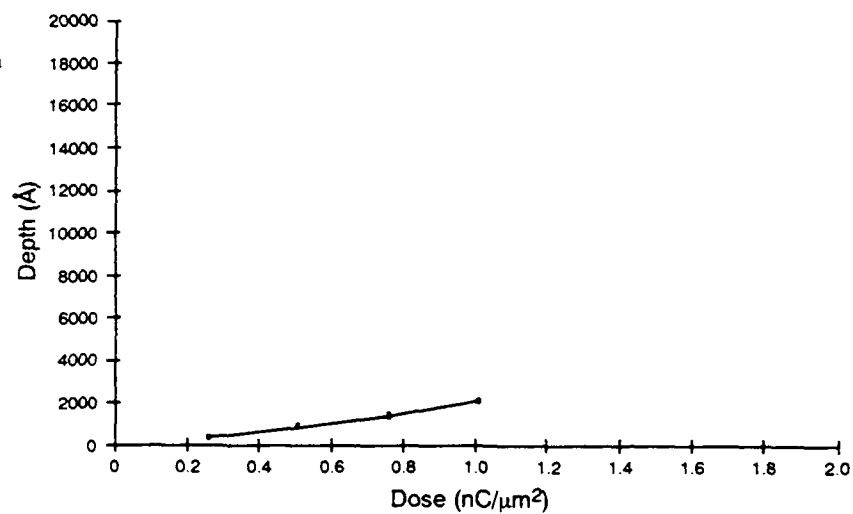
Figure 11. Depth versus dose for gold.

Depth (Å) vs Dose (nC/μm²)

- evaporated gold
- sputtered gold

12

Figure 12. Rate versus dose for gallium arsenide.

Rate (μm³/s) versus Dose (nC/μm²)

- 0.450 pA
- 0.366 pA

Figure 13. Rate versus dose for 28-percent aluminum gallium arsenide.

Rate (μm³/s) versus Dose (nC/μm²)

- 0.450 pA
- 0.366 pA

Figure 14. Rate versus dose for polysilicon.

Rate (μm³/s) versus Dose (nC/μ m²)
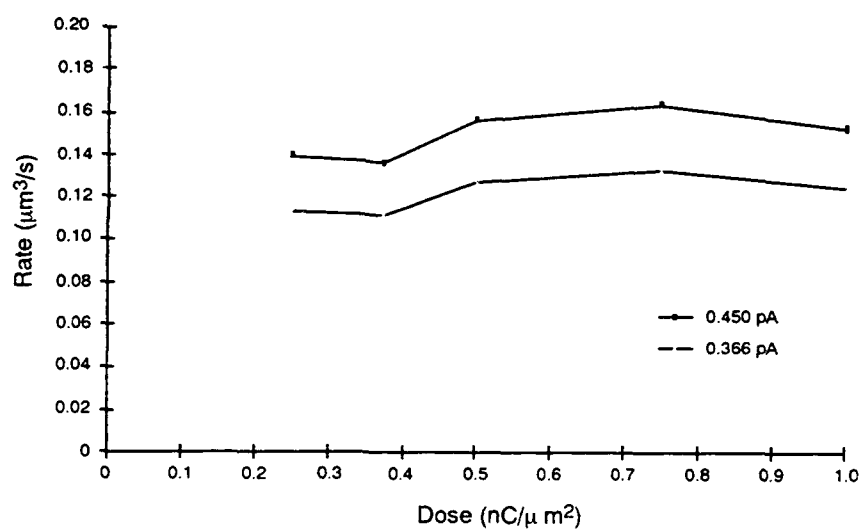
- 0.450 pA
- 0.366 pA

13

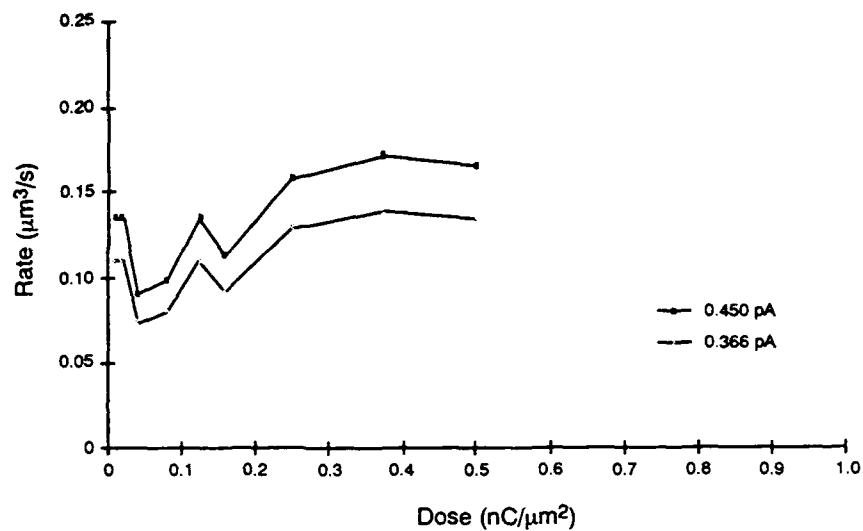**Figure 15. Rate versus dose for silicon dioxide.**

Figure 16. Rate versus dose for silicon carbide.
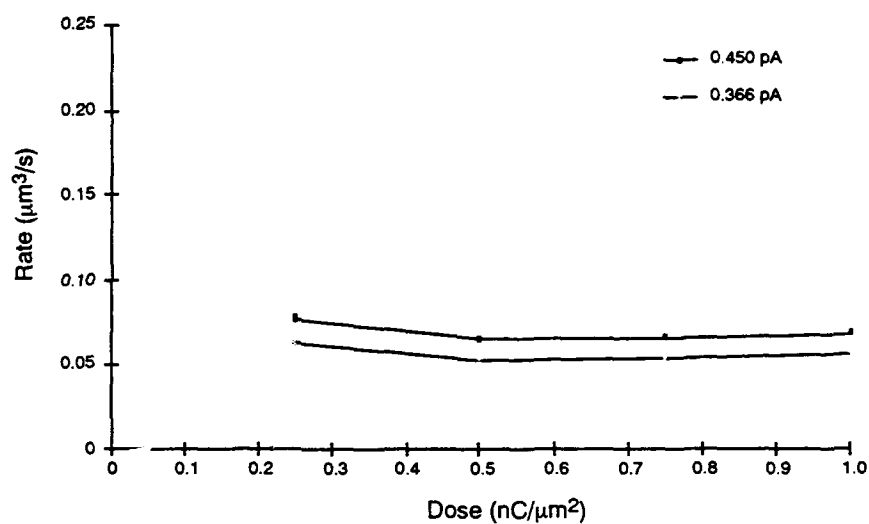
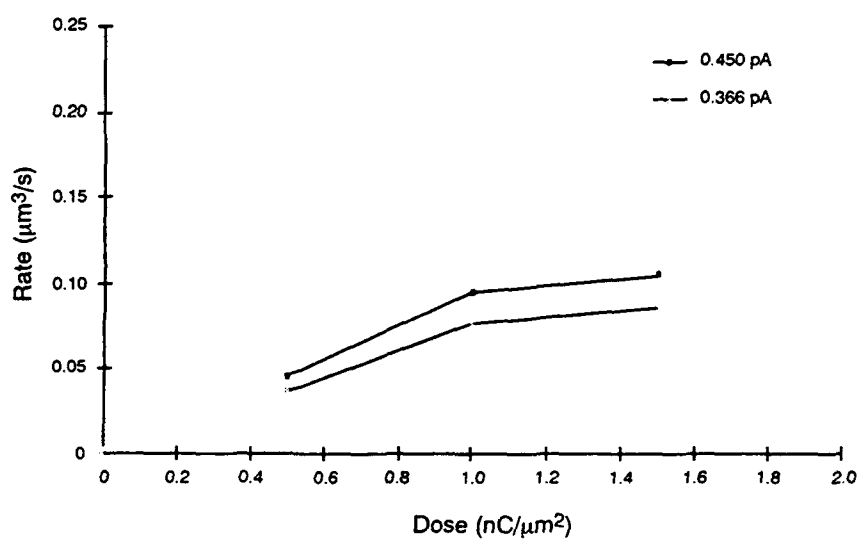**Figure 17. Rate versus dose for barium titanate.**
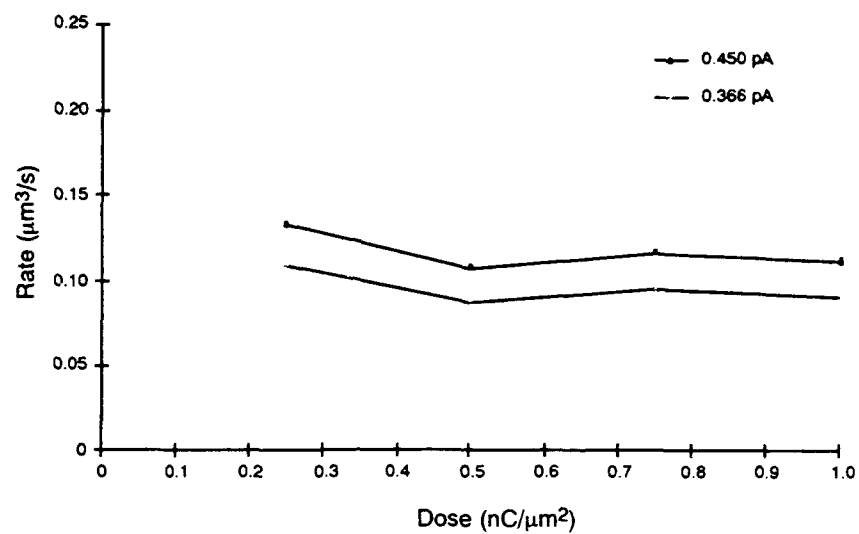

14

Figure 18. Rate versus dose for evaporated aluminum.

Rate (μm³/s) vs Dose (nC/μm²)

Legend: 0.450 pA, 0.366 pA

Figure 19. Rate versus dose for e-beam deposited aluminum.

Rate (μm³/s) vs Dose (nC/μm²)

Legend: 0.450 pA, 0.366 pA
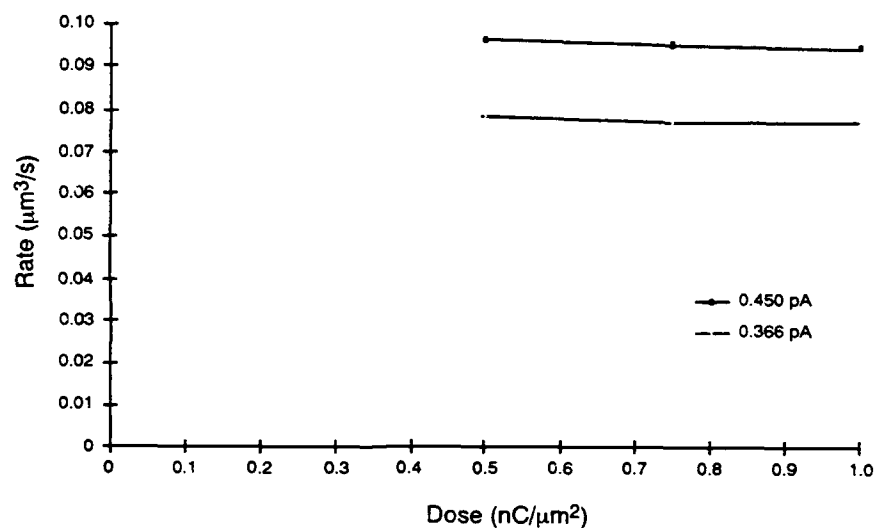
Figure 20. Rate versus dose for silicon nitride.

Rate (μm³/s) vs Dose (nC/μm²)
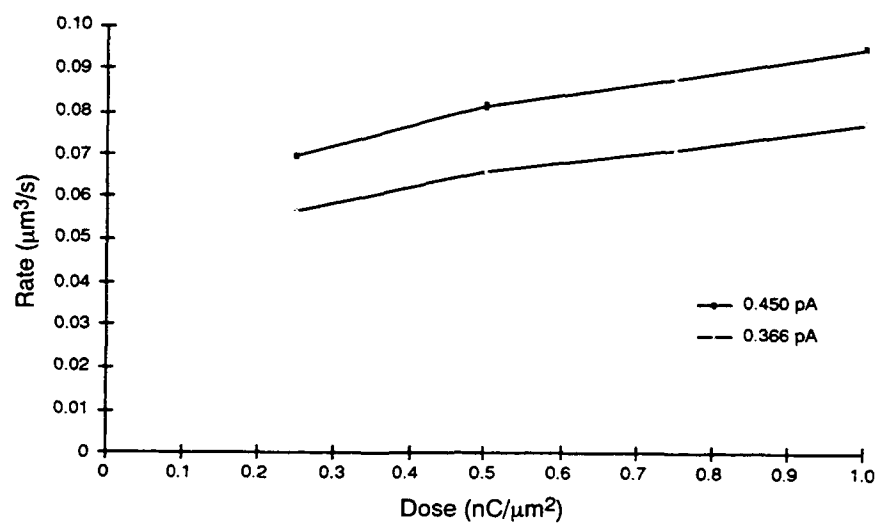
Legend: 0.450 pA, 0.366 pA

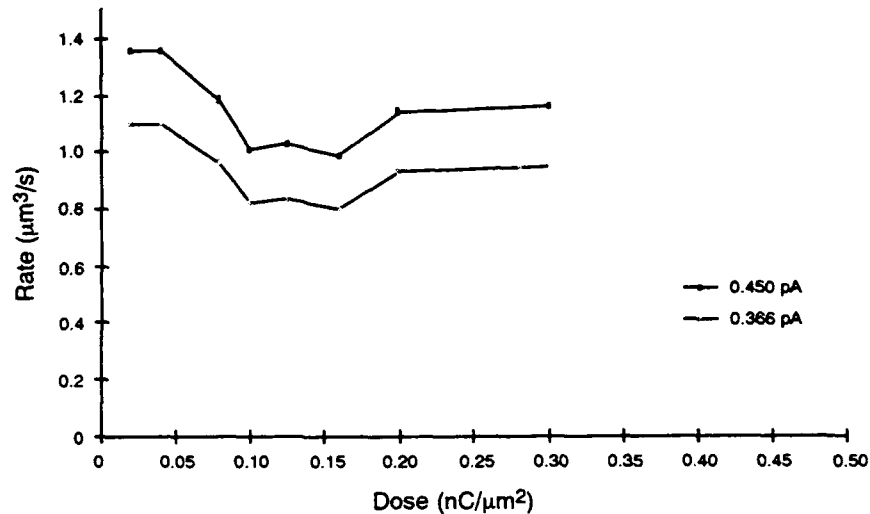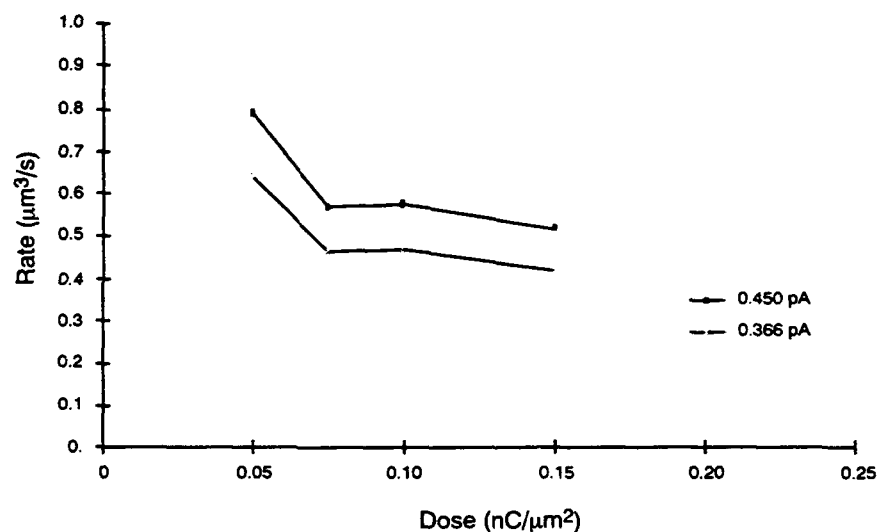**Figure 21. Rate versus dose for sputtered gold.**

Figure 22. Rate versus dose for evaporated gold.

4. Conclusions

The data obtained from this research show that each material has a specific material removal rate. Of the materials tested, gold milled the fastest; this indicates that the atomic weight of the material does not play a significant role in the removal process. Gold, which has an atomic weight of 196.9665, is milled at a rate of 0.8891 $\mu m^3/nC$, while silicon carbide, which has an atomic weight of 32.0855, mills at a rate of 0.1452 $\mu m^3/nC$. The milling rate of the test material correlates with the sputter etch characteristics of the material. When a material is impacted by the gallium ion, the kinetic energy of the ion breaks apart the bonds of the material if the energy of the ion is greater than the binding energy of the material. The energy necessary to break the bonds of the material, or threshold energy, is between 5 and 40 eV. The other factor affecting the sputter rate of the material is the angle of incidence of the ion beam. For most materials, the highest sputter etch rate occurs when the angle of incidence is 45° from the normal. For the

data presented here, all milling was done at normal incidence. For gold, the highest sputter etch rate occurs at 0° angle of incidence and decreases as the angle increases.[2] This explains why the gold, with the highest atomic weight, still etches the fastest of all the materials tested.

For most of the materials tested, the depth-to-dose data we obtained correlated very well with a straight line. This correlation allows linear approximation for dose values at a given depth. For some of the materials we tested, the calculated y intercept was more than 100 Å above or below the zero point. This effect could be caused by several factors. At low dose levels, the ions are being implanted into the surface rather than removing any material. This low-dose effect is more pronounced with a material such as barium titanate, which has a very slow mill rate. The other possible cause of this non-linearity is the profilometer accuracy for very small step heights. In the case of the evaporated gold, the mill rates are so high that small depths cannot be easily milled into the surface. This causes a lack of data at the smaller doses. The slope and y values of the linear approximation are given in table 2. Table 2 also shows the average mill rate for a material at a given beam current. The data in this table will help in the calculation of dose or depth values and milling time for a given material.

For those wishing to use the FIB milling capability available at the semiconductor electronics materials technology facility, these data will allow them to determine the time and dose required to mill their samples.

Acknowledgments

---

[2]David J. Elliott, *Integrated Circuit Fabrication Technology*, McGraw-Hill, Inc. (1982).

Distribution

Administrator
Defense Technical Information Center
Attn: DTIC-DDA (2 copies)
Cameron Station, Building 5
Alexandria, VA 22304-6145

US Army Electronics Technology & Devices
  Laboratory
Attn: SLCET-E
Attn: SLCET-ER
Attn: SLCET-ER-S
Attn: SLCET-I, Microelectronics
Attn: SLCET-IA
Attn: SLCET-D, Electronic Tech & Devices Lab
FT Monmouth , NJ 07703-5601

Under Secretary of Defense for Research &
  Engineering
Attn: Research & Advanced Tech
Attn: Asst to Sec/Atomic Energy
Attn: Dept Asst Sec/Energy Environment &
  Safety
Attn: Dep Under Sec/Res & Advanced Tech
Attn: Dep Under Sec/Test & Evaluation
Department of Defense
Washington, DC 20301

Commander
US Army Materiel Command
Attn: AMCDE, Dir for Dev & Engr
Attn: AMCDE-R, Sys Eval & Testing
Attn: AMCNC, Nuclear-Chemical Ofc
5001 Eisenhower Ave
Alexandria, VA 22333-0001

Commander
CECOM R&D Tech Library
Attn: ASQNC-ELC-IS-L-R
FT Monmouth, NJ 07703-5018

Director
US Army Electronic Warfare Laboratory,
  LABCOM
Attn: ASQNC-ELC-IS, Information Services
  Div
FT Monmouth, NJ 07703-5601

Director
US Army Research Laboratory
Attn: SLCBR-AM
Attn: SLCBR-TB-VL
Attn: SLCBR-X
Attn: SLCBR
Aberdeen Proving Ground, MD 21005-5066

Naval Research Laboratory
Attn: Code 2620, Tech Library Br
Washington, DC 20375

Commander
Naval Surface Warfare Center
Attn: Code WA501, Navy Nuc Prgms Ofc
Attn: Code WA52
Attn: Microelectronics, R. Goetz
Attn: E-43, Technical Library
Attn: WA50
White Oak, MD 20910

Commander
Naval Surface Warfare Center
Attn: Code WR, Research & Technology Dept
Attn: DX-21 Library Div
Dahlgren Laboratory
Dahlgren, VA 22448

Booz-Allen & Hamilton, Inc
Attn: J. Terrell
8283 Greensboro Drive
McLean, VA 22102

Micrion Corporation
Attn: D. Stewart
One Corporation Way, Centennial Park
Peabody, MA 01960-7990

U.S. Army Research Laboratory
Attn: AMSRL-D-C, Legal Office
Attn: AMSRL-OP-CI-AD, Library (3 copies)
Attn: AMSRL-OP-CI-AD, Mail & Records
  Mgmt
Attn: AMSRL-OP-CI-AD, Tech Pub
Attn: AMSRL-EP-EE, G. Simonis
Attn: AMSRL-EP-EE, M. Stead
Attn: AMSRL-SL-NC, J. McCullen

Distribution (cont'd)

US Army Research Laboratory (cont'd)
Attn: AMSRL-SS-F, R. B. J. Goodman
Attn: AMSRL-SS-IA, T. Tayag
Attn: AMSRL-SS-IA, N. Gupta
Attn: AMSRL-WT-CS, Chief
Attn: AMSRL-WT-E, Chief
Attn: AMSRL-WT-EH, Chief
Attn: AMSRL-WT-EP, Chief
Attn: AMSRL-WT-ES, Chief
Attn: AMSRL-WT-L, R. Gilbert
Attn: AMSRL-WT-N, J. M. McGarrity
Attn: AMSRL-WT-NB, D. Davis
Attn: AMSRL-WT-ND, J. R. Miletta
Attn: AMSRL-WT-NG, A. J. Lelis
Attn: AMSRL-WT-NG, B. Geil (15 copies)
Attn: AMSRL-WT-NG, B. J. Rod
Attn: AMSRL-WT-NG, B. McLean
Attn: AMSRL-WT-NG, C. Pennise

US Army Research Laboratory (cont'd)
Attn: AMSRL-WT-NG, Chief
Attn: AMSRL-WT-NG, H. Boesch
Attn: AMSRL-WT-NG, Harvey Eisen
Attn: AMSRL-WT-NG, J. Benedetto
Attn: AMSRL-WT-NG, K. W. Bennett
Attn: AMSRL-WT-NG, M. DeLancey
Attn: AMSRL-WT-NG, R. B. Reams
Attn: AMSRL-WT-NG, R. Moore
Attn: AMSRL-WT-NG, T. Griffin
Attn: AMSRL-WT-NG, T. Mermagen
Attn: AMSRL-WT-NG, T. Oldham
Attn: AMSRL-WT-NG, T. Taylor
Attn: AMSRL-WT-NH, H. Brandt
Attn: AMSRL-WT-P, Chief
Attn: AMSRL-WT-RS, Chief
Attn: AMSRL-WT-TN, Chief
Attn: AMSRL-WT-TS, Chief